5-1-2023

Blockade of TRPV channels by intracellular spermine

Grigory Maksaev
Washington University School of Medicine in St. Louis

Peng Yuan
Washington University School of Medicine in St. Louis

Colin G Nichols
Washington University School of Medicine in St. Louis

Recommended Citation

ARTICLE

Blockade of TRPV channels by intracellular spermine

Grigory Maksaev[1] , Peng Yuan[1], and Colin G. Nichols[1]

The Vanilloid thermoTRP (TRPV1–4) subfamily of TRP channels are involved in thermoregulation, osmoregulation, itch and pain perception, (neuro)inflammation and immune response, and tight control of channel activity is required for perception of noxious stimuli and pain. Here we report voltage-dependent modulation of each of human TRPV1, 3, and 4 by the endogenous intracellular polyamine spermine. As in inward rectifier K channels, currents are blocked in a strongly voltage-dependent manner, but, as in cyclic nucleotide-gated channels, the blockade is substantially reduced at more positive voltages, with maximal blockade in the vicinity of zero voltage. A kinetic model of inhibition suggests two independent spermine binding sites with different affinities as well as different degrees of polyamine permeability in TRPV1, 3, and 4. Given that block and relief occur over the physiological voltage range of action potentials, voltage-dependent polyamine block may be a potent modulator of TRPV-dependent excitability in multiple cell types.

Introduction

ThermoTRPV (TRPV1–4) channels are non-selective, Ca^{2+}-permeable, cationic channels gated by a variety of stimuli, including noxious heat (which is reflected in their classification as "thermo"), pH, natural plant-derived compounds (such as capsaicin and cannabinoids), endogenous ligands, and synthetic drugs (Yuan, 2019). They are involved in a variety of sensory functions, including thermo- and pain sensation, and dysfunction of these channels underlies multiple diseases, ranging from various kinds of pain and hyperalgesia (TRPV1; Patapoutian et al., 2009; Marrone et al., 2017) to immune system-related diseases (TRPV2; Perálvarez-Marín et al., 2013), chronic itch and skin Olmsted syndrome (TRPV3; Nilius et al., 2014), and neurological and musculoskeletal disorders (TRPV4; White et al., 2016; Deng et al., 2018), for many of which there is no therapy. Among TRPVs, TRPV1 exhibits a very clear voltage dependence (Caterina et al., 1997; Tominaga et al., 1998), although, unlike canonical voltage-sensitive channels, the S4 helix does not serve as a voltage sensor, and the mechanism of TRPV1 voltage dependence is not well understood (Yang et al., 2020). While current pharmacology of TRPVs is quite extensive, there is still a need to identify novel regulatory mechanisms that could be exploited for more granular and fine-tuning of thermoTRPV activity.

The natural polyamines (PAs) putrescine, spermidine, and spermine, are small organic cations, present in sub-millimolar concentrations in the cytoplasm of virtually all cells and in the extracellular fluid, and have long been recognized as critical for cell growth and proliferation (Pegg, 2016; Igarashi and Kashiwagi, 2019). Intracellular PA levels decrease with age, while pathological alterations of PA levels affect cognitive functions and have been linked to brain ageing and degeneration (Minois et al., 2011; Skatchkov et al., 2014, 2016; Saiki et al., 2019; Sánchez-Jiménez et al., 2019), as well as to cancer (Casero et al., 2018; Li et al., 2020). Other well-studied PA functions are regulation of protein expression via interaction with DNA and RNA molecules (Dever and Ivanov, 2018) and modulation of ion channels, including inward-rectifier potassium (Kir) channels (Lopatin et al., 1994; Méndez-González et al., 2016), cyclic nucleotide-gated channels (Lu and Ding, 1999; Guo and Lu, 2000), ionotropic glutamate receptors (Bowie and Mayer, 1995; Bähring et al., 1997; Bowie et al., 1998; Twomey et al., 2018), and voltage-gated Na^+ channels (Fleidervish et al., 2008).

TRPVs are widely expressed in excitable membranes of neurons of brain, central and peripheral nervous systems, pancreatic β-cells, and cardiomyocytes, and tight control of channel activity is critical for perception of noxious stimuli and pain. Thus, TRPVs are promising therapeutic targets for human pain conditions. There have been several isolated reports of voltage-dependent PA inhibition of TRP channel family members, including TRPC4 (Kim et al., 2016, 2020), TRPM4 (Nilius et al., 2004), and TRPM7 (Zhelay et al., 2018). It has also been shown that extracellular spermine permeates, potentiates, and weakly activates TRPV1 channels (Ahern et al., 2006), but the effects of intracellular PAs on TRPV sub-family members remain unexplored. Here, we characterize the voltage-dependent inhibition

[1]Department of Cell Biology and Physiology, Center for Investigation of Membrane Excitability Diseases, Washington University School of Medicine, St. Louis, MO, USA.

Correspondence to Grigory Maksaev: gmaksaev@wustl.edu

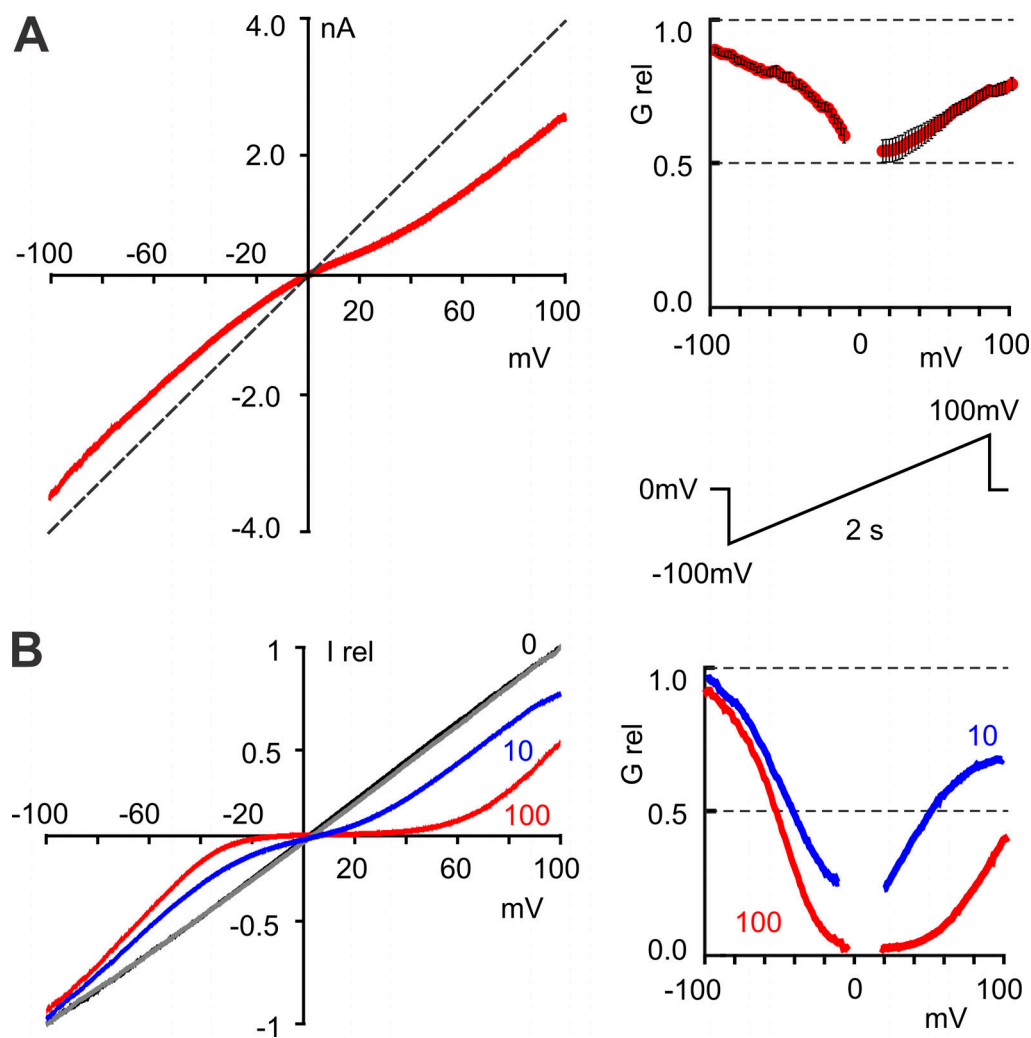P. Yuan's current affiliation is Icahn School of Medicine at Mount Sinai, New York, NY, USA.

Figure 1. **Inhibition of hTRPV3 channel by intracellular factors. (A)** Representative ramp I-V relationship of hTRP3 (red) measured in on-cell patches from a COSm6 cell, transiently expressing hTRPV3. Dashed line is presented for a reference and represents a linear slope. The agonist 2-APB was present in the pipette. Inset: Normalized voltage dependence of the patch conductance (n = 9, ± SE, top) and a voltage ramp protocol used (bottom). **(B)** Representative normalized I (G_{rel})-V relationships for 2-APB-activated currents, measured in inside-out patches from COSm6 cells, transiently expressing hTRPV3. Gray and blue, in absence and presence of 10 µM cytoplasmic spermine, respectively; black and red, in absence and presence of 100 µM cytoplasmic spermine, respectively. Inset: G_{rel}-V relationship for currents at left, in the presence of 10 or 100 µM spermine.

of TRPVs by intracellular polyamines. The data reveal a strong, physiologically relevant action that varies in potency between sub-family members, pointing to the possibility of developing channel-selective modulators of this inhibition.

Materials and methods

Channel constructs

The experiments were performed on cloned full-length human TRPV1 (Caterina et al., 1997), TRPV3 (Peier et al., 2002; Smith et al., 2002), and TRPV4 (Liedtke et al., 2000; Strotmann et al., 2000) channels in pV10 mammalian expression vector with a C-terminal EGFP tag.

Electrophysiology

COSm6 cells were transfected with human full-length TRPV1, TRPV3, or TRPV4 plasmids in pV10-EGFP vector. Briefly, 0.5 µg

of plasmid and 1.5 µl of FuGENE6 reagent (Promega) were added to 100 µl of OPTI-MEM media (Gibco) and incubated for 25–30 min at room temperature. The mixture then was dropwise added to a 35 mm Petri dish, containing COSm6 cells (~50–60% confluency) in 2 ml of DMEM media (Gibco), supplemented with 10% FBS (Gibco) and penicillin/streptomycin (Sigma-Aldrich). The cells were used for patch-clamping 24–48 h after transfection. Protein expression was assessed via EGFP tag fluorescence imaging. Cell-attached patches were formed, and inside-out membrane patches were excised from cellular plasma membranes using glass pipettes (2502; Kimble Chase) with ~2 MΩ resistance, fabricated with a Sutter P-96 puller (Sutter Instruments). Symmetric high potassium solutions (148 mM KCl, 1 mM EGTA, 1 mM K_2EDTA, and 10 mM HEPES, pH 7.38) were present in both patch and bath solutions. To activate all channels present in patches, specific agonists at saturating concentrations (1 mM 2-APB for TRPV1 and TRPV3, or 50 nM GSK101 for
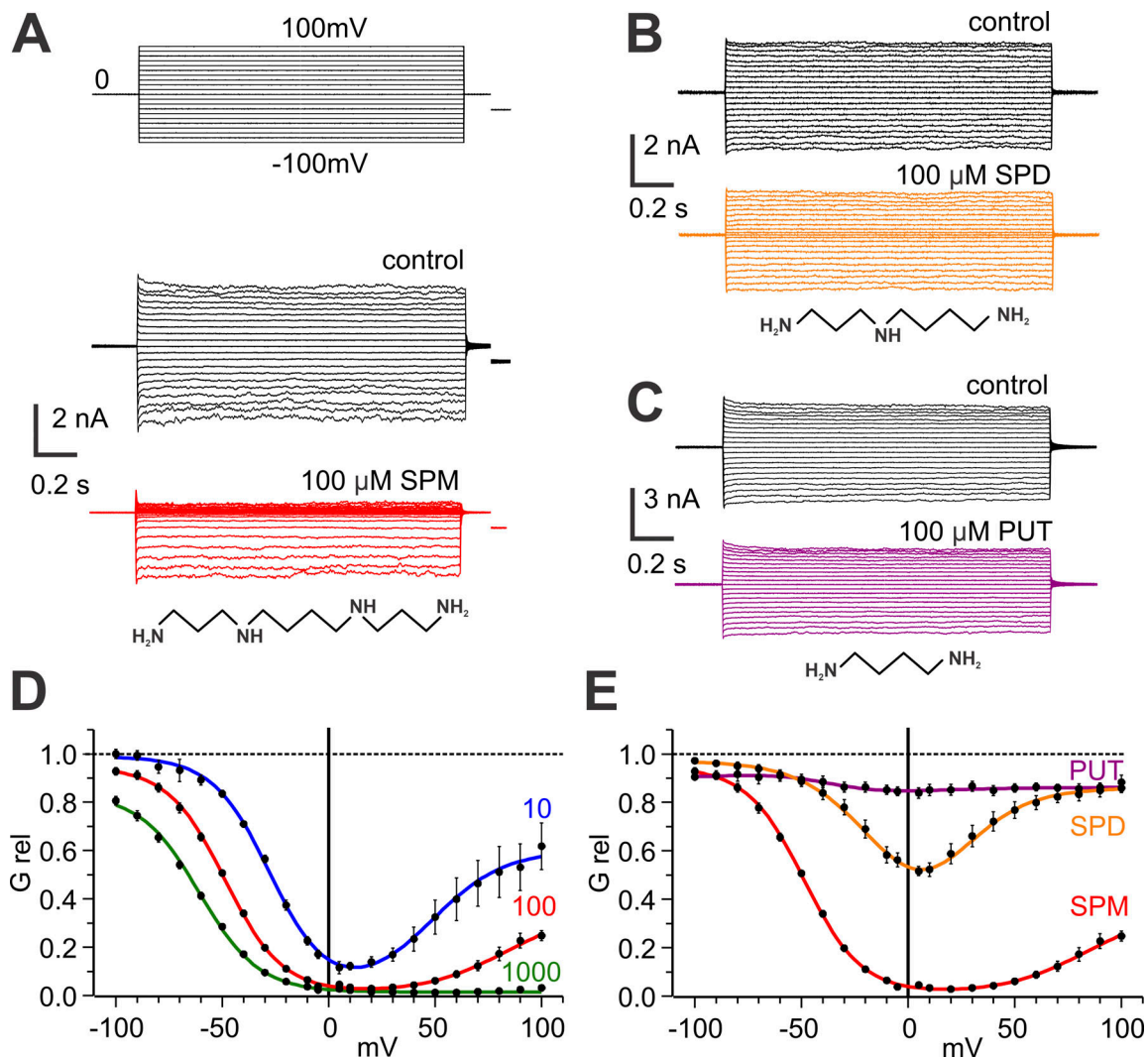
Figure 2. Polyamine block of hTRPV3 is concentration- and charge-dependent. (A) Representative traces of the 2-APB-induced hTRPV3 currents, measured using a voltage step protocol (top) in absence (center, black) and presence of 100 μM cytoplasmic spermine (SPM, bottom, red). **(B and C)** Representative traces of 2-APB-induced hTRPV3 currents, measured using a voltage step protocol as in A in absence (black) and presence of 100 μM cytoplasmic polyamine spermidine (SPD; B) or putrescine (PUT; C). **(D)** Averaged (n = 5, ± SE) G_{rel}-V relationships for hTRPV3 in presence of 10 (blue line), 100 (red line), and 1,000 μM (green line) cytoplasmic spermine, from recordings as in A. **(E)** Averaged (n = 5, ± SE) G_{rel}-V relationships for hTRPV3 in presence of cytoplasmic 100 μM spermine (SPM, red line), 100 μM spermidine (SPD, orange line), and 100 μM putrescine (PUT, purple line). All datasets were fitted with the sum of two Boltzmann distributions.

TRPV4) were applied to cell-attached patches in the patch pipette solution (TRPV3, Fig. 1 A), or to inside-out membrane patches from the cytoplasmic side via continuous bath perfusion (TRPV1, 3, and 4). Relative conductance in presence of polyamines (putrescine, spermidine, spermine, or NASPM) in the same excised inside-out patches was assessed by further bath perfusion with the same buffer solution, containing both respective saturating agonist and polyamine at indicated concentrations (Figs. 2, 4, and 6). Currents, induced in patches by the agonists and/or agonist–polyamine mixtures, were measured in response to the linear –100 to 100 mV 2-s-long voltage ramps (I-V relationships, Fig. 1 A) and a 2-s-long –100 to 100 mV (with a 10 mV increment) voltage step protocol (G_{rel}-V relationships, Figs. 2, 4, and 6). The data were acquired with Axopatch-1D patch-clamp amplifier and Digidata 1320 digitizer (Axon

Instruments) at 3 kHz and low-pass filtered at 1 kHz. Initial data analysis was performed in pClamp 10.7 software suite (Molecular Devices). G_{rel}-V relationships for all polyamines (Figs. 2, 3, and 4) represent the average data (five individual patches per data point ± SE) and for each channel and each polyamine concentration were independently fit using QtiPlot data analysis suite (Ion Vasilief, https://www.qtiplot.com) with a sum of two (ascending and descending) Boltzmann distributions:

$$G_{rel}(V) = G_1^{min} + (G_1^{max} - G_1^{min})/$$
$$\{1 + \exp[Z_1 * 0.03963 * (V_1^{mid} - V)]\}$$
$$+ G_2^{min} + (G_2^{max} - G_2^{min})/$$
$$\{1 + exp[Z_2 * 0.03963 * (V - V_2^{mid})]\},$$

where G^{min} and G^{max} are minimal and maximal conductances, Z_1 and Z_2 are gating charges, V^{mid} is a mid-point potential, and V is a membrane potential.

Modeling

Data presented in Fig. 6 were fit using Microsoft Excel Solver independently for each channel assuming the same values for all parameters (six for a two-site model and four for a simplified one-site model) for each polyamine concentration. Fitting was performed via minimization of RMSD between experimental data and fitting curve using the equation presented on Fig. 5 C.

TRPV3 pore structure (presented in Fig. 5 A) was generated with VMD suite (Humphrey et al, 1996). Pore electrostatic profiles (presented in Fig. 5 D) were generated with MOLEonline Server (https://mole.upol.cz) and UCSF ChimeraX 1.5 suite (Pettersen et al., 2021).

Results

TRPV3 is inhibited by cytoplasmic spermine

When expressed in COSm6 cells and activated in cell-attached patches by the TRPV3-specific agonist 2-APB (present at 1 mM in the patch pipette), recombinant C-terminal EGFP-tagged TRPV3 typically elicited large currents, up to a few nanoamps per patch. In our initial studies, we first observed a consistent kink in cell-attached current-voltage relationships around the reversal potential (Fig. 1 A). TRPV3-specific conductance, measured in response to a linear 2 s long voltage ramp (–100 to 100 mV), decayed in the vicinity of 0 mV and recovered at higher de- and hyper-polarizing potentials (Fig. 1 A), which hinted at a potential voltage-dependent inhibition by intracellular factors around 0 mV. As previous studies indicated, inhibition of multiple types of channels, including a few other TRP family members, by intra-cellular polyamines, we tested the effect of the intracellular polyamine spermine on human TRPV3 channel activity. Following patch excision, TRPV3 currents rapidly linearized, losing the kink in the I-V curve around 0 mV (Fig. 1 B). Application of spermine to the cytoplasmic side of inside-out patches at 10 or 100 µM restored a kink, and I-V and G_{rel}-V curves (Fig. 1 B) became qualitatively similar to those obtained in cell-attached configuration (Fig. 1 A), suggesting that endogenous polyamines, or other organic cations, inhibit the channel in the intact cell.

We examined TRPV3 conductance in excised patches in the presence of 10, 100, and 1,000 µM spermine or of the shorter polyamines spermidine and putrescine at 100 µM (Fig. 2). The ratio of TRPV3 currents in the presence versus absence of spermine (G_{rel}) was used as a measure of efficiency and voltage-
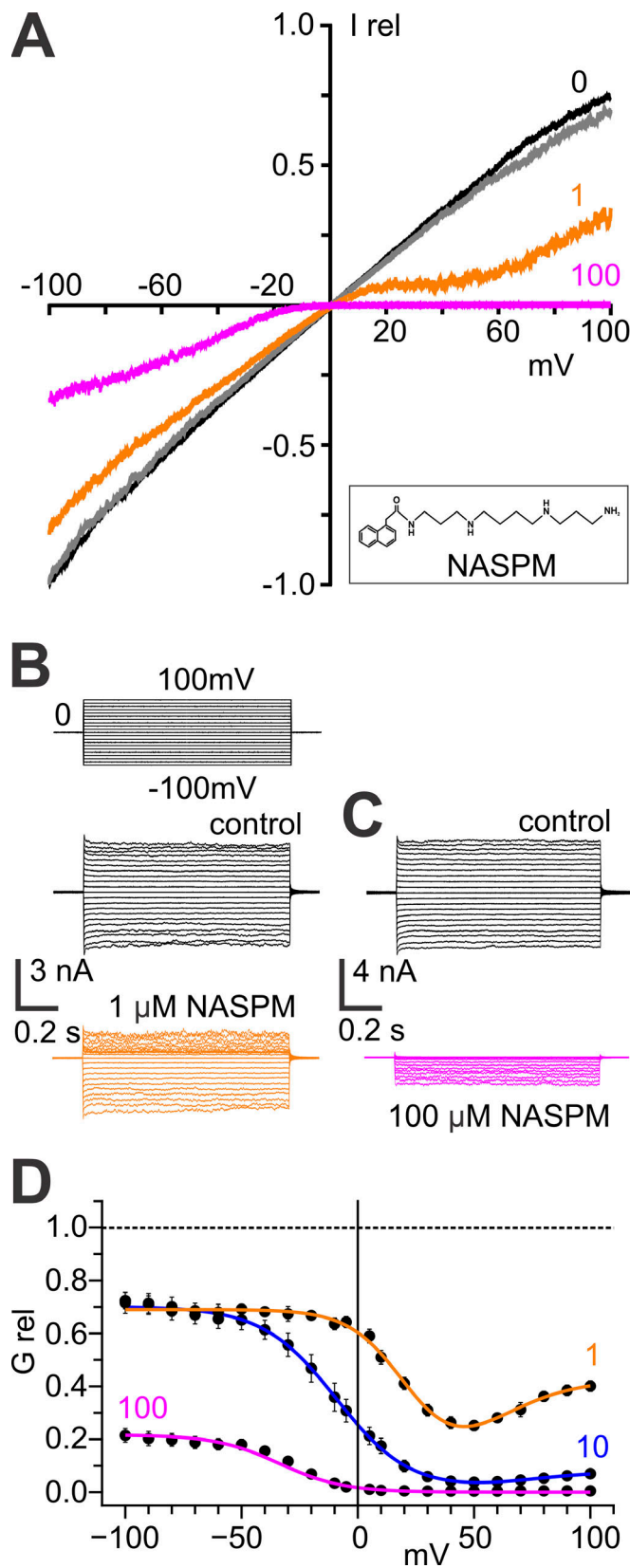

Figure 3. **Inhibition of hTRPV3 channel by intracellular NASPM.** **(A)** Representative normalized ramped I-V relationships for 2-APB-activated currents, measured in inside-out patches from COSm6 cells, transiently expressing hTRPV3. Gray and orange, in absence and presence of 1 µM cytoplasmic NASPM, respectively; black and pink, in absence and presence of 100 µM cytoplasmic NASPM, respectively. **(B)** Representative traces of the 2-APB-induced hTRPV3 currents, measured using a voltage step protocol (top) in absence (center, black) and presence of 1 µM cytoplasmic NASPM (bottom, orange). **(C)** Representative traces of 2-APB-induced hTRPV3 currents, measured using a voltage step protocol as in B in absence (black) and presence (pink) of 100 µM cytoplasmic NASPM. **(D)** Averaged (n = 5, ± SE) G_{rel}-V relationships for hTRPV3 (in excised patches) in presence of cytoplasmic 1 µM (orange), 10 µM (blue), and 100 µM (pink) NASPM. All datasets were fitted with the sum of two Boltzmann distributions.

Maksaev et al.
Blockade of TRPV channels by intracellular spermine

Journal of General Physiology
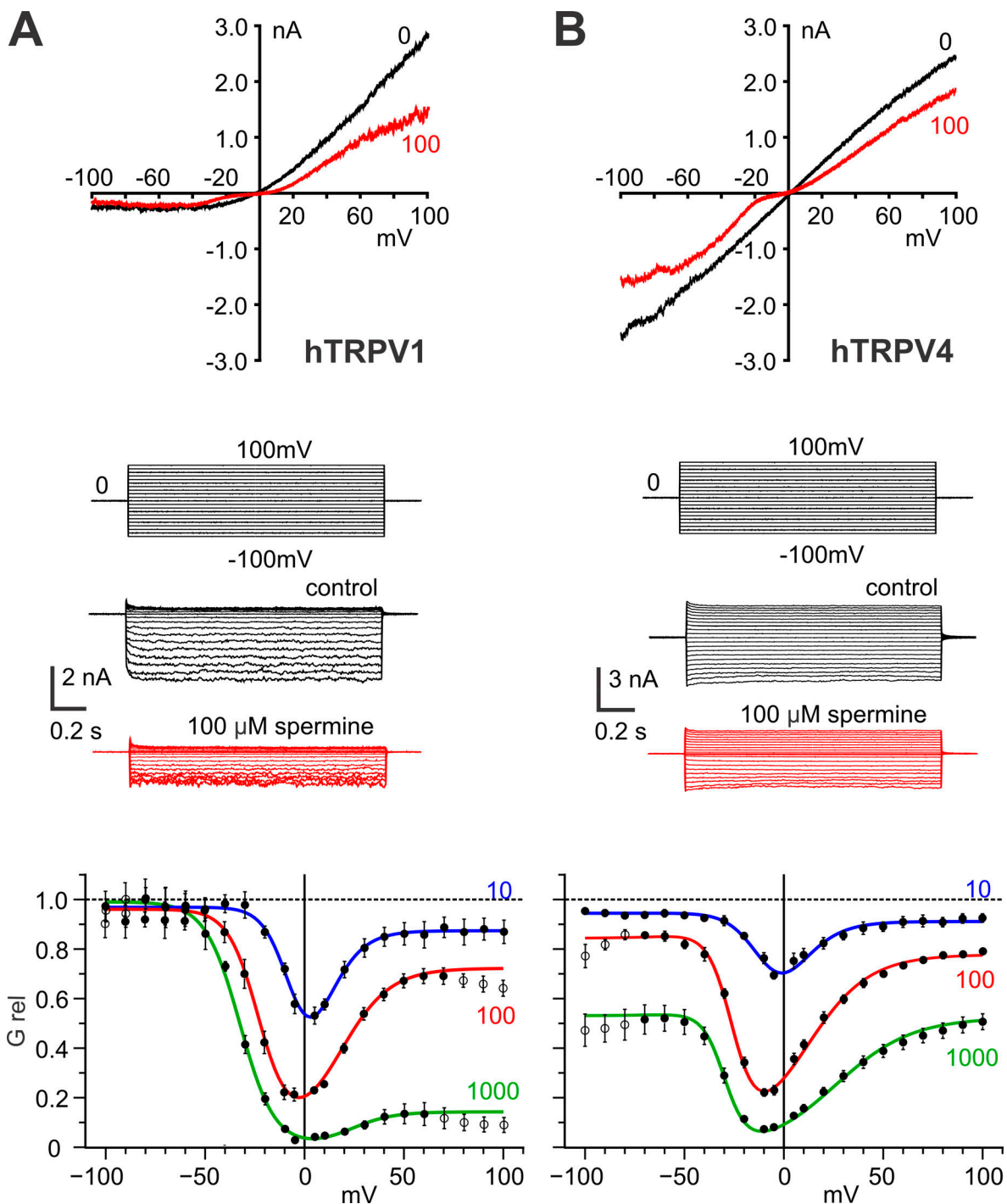https://doi.org/10.1085/jgp.202213273

4 of 11

Figure 4. Inhibition of hTRPV1 and hTRPV4 channels by spermine. (A and B) Top: Ramped I-V relationships for human TRPV1 (A) and TRPV4 (B) channels in the absence (black) and presence (red) of 100 µM intracellular spermine. The currents were induced by saturating concentrations of agonists: 2-APB (TRPV1) and GSK101 (TRPV4) prior to addition of spermine. Middle: Representative traces of agonist-induced hTRPV1 (A) and hTRPV4 (B), measured using a voltage step protocol (top) in absence (black) and presence (red) of 100 µM cytoplasmic spermine, respectively. Bottom: Averaged (n = 5, ± SE) G_{rel}-V relationships for hTRPV1 and hTRPV4 channels in excised patches measured using the step protocol in presence of 10 µM (blue), 100 µM (red), or 1,000 µM (green) intracellular spermine. The datasets were fitted with the sum of two Boltzmann distributions, the data points labeled as empty circles were excluded from the fitting. Fitting results are presented in Table 1.

dependence of spermine inhibition (Fig. 1). Inhibition of TRPV3 channels by spermine was clearly concentration-dependent (Fig. 2, A and D). Spermidine also inhibited TRPV3 channels in excised inside-out patches (Fig. 2, B and E) with similar

characteristics, although compared to spermine, the inhibition was less potent (Fig. 2 E). The effect of 100 µM intracellular putrescine was negligible (Fig. 2, C and E). Overall, these observations are in line with data on natural polyamine block of

Table 1. Results of fitting of the G_{rel}-V relationships for TRPV1, 3, and 4 with a sum of two Boltzmann distributions for spermine inhibition (presented in Fig. 2 D and Fig. 4)

Spermine, µM	V_{mid1}, mV	V_{mid2}, mV	Z_1, e	Z_2, e
TRPV1				
10	−6.7	7.7	−3.6	−2.7
100	−22.9	17.1	−3.3	−2.0
1,000	−32.5	22.8	−2.9	−2.4
TRPV3				
10	−27.5	50.6	−1.9	−1.3
100	−48.9	82.5	−1.8	−1.3
1,000	−62.3	-	−1.7	-
TRPV4				
10	−11.9	−3.5	−2.8	−2.1
100	−26.1	9.7	−4.1	−1.6
1,000	−29.9	25.9	−4.5	−1.3

TRPV3 in presence of 1 mM spermine was fitted with only one (descending) Boltzmann distribution.

Kir channels (Lopatin et al., 1994, 1995; Nichols and Lee, 2018; Lee and Nichols, 2023) and of CNG channels (Lu and Ding, 1999; Guo and Lu, 2000). In the latter, there is good evidence that spermine acts as a permeant blocker, and that relief of block at positive voltages is due to voltage-driven permeation of spermine to the extracellular side of the membrane. To examine the possibility that a similar mechanism underlies relief of TRPV3 inhibition at positive voltages, we tested the effect of the AMPAR antagonist (Koike et al., 1997; Twomey et al., 2018), 1-naphthyl-acetyl spermine (NASPM). NASPM is a spermine analog, with a bulky aromatic group at one end of the molecule (Fig. 3 A, inset). At 100 µM, NASPM also exhibited strong voltage-dependent inhibition at negative potentials but, in contrast to the natural polyamines, the block was not relieved at positive potentials (Fig. 3). At 10 µM and more so at 1 µM, however, there was clear evidence of relief at the most positive potentials (Fig. 3, A and D), which suggests weak permeation. Given that the head group is too large to permeate the TRPV pore resolved in static cryo-EM structures (Singh et al., 2018; Zubcevic et al., 2018a; Deng et al., 2020), this would suggest that there may be plasticity of the TRPV3 selectivity filter, as previously suggested (Ferreira and Faria, 2016) for TRPV1 (Chung et al., 2008) and TRPV2 (Zubcevic et al., 2018b).

Inhibition of other thermoTRPVs by intracellular polyamines
We then characterized the action of the most potent of the natural PAs, spermine, on human TRPV1 and TRPV4 (Fig. 4, A and B), using the same stepped voltage protocol as above. Owing to lack of high potency agonists, we did not evaluate polyamine inhibition of human TRPV2 (Juvin et al., 2007; Neeper et al., 2007). In excised patches, agonist-activated I-V relationships for excised TRPV4 were again almost linear, without noticeable rectification at either positive or negative

membrane potentials (Fig. 4 B), whereas TRPV1 demonstrated a strong outward rectification (Fig. 4 A), in agreement with previous findings (Yang et al., 2020). Independent of this intrinsic outward rectification, spermine added to the cytoplasmic side at concentrations 10, 100, and 1,000 µM caused a similar inhibition of both hTRPV1- and hTRPV4-specific currents, again with a maximum efficacy near the reversal potential (Fig. 4, A and B).

Inhibition of each of TRPV1, 3, and 4 channels by intracellular spermine was rapid, with no measurable time-dependence, and shared similar voltage- and concentration-dependence, with most efficient blocking occurring around the reversal potential, resulting in the characteristic "dip" on the G_{rel}-V relationship (Fig. 1 B, Fig. 2 D, and Fig. 4). Inhibitory potency was not identical, the rank order being most potent for TRPV3, less so for TRPV1, and weakest for TRPV4. Fitting of G_{rel}-V plots with the sum of two Boltzmann distributions (Fig. 2 D and Fig. 4) also revealed the strongest concentration-dependent shift of midpoint potential (V_{mid}) for TRPV3 (Table 1). For each channel subtype, inhibition by 100 µM spermine was marginal to moderate at what would be a typical cellular resting membrane potential (−70 mV), but inhibition was ~80–90% for each channel at around 0 mV, which would effectively inhibit nonselective cationic TRPV currents during the depolarization phase of an action potential.

A two-site kinetic model can account for spermine block and relief
Thus, PA inhibition of thermoTRPVs, similarly to Kir channels and especially to CNG channels, is voltage and concentration dependent, and follows the same dependence on the length/charge of PAs. The voltage-dependence implies a binding site within the electric field deep in the TRPV pore, potentially at the selectivity filter or in the cytoplasmic cavity (Fig. 5 A). Another hallmark of PA inhibition of thermoTRPVs, particularly obvious in the case of TRPV1, is a clear second descending phase for all spermine concentrations (Figs. 4 and 6), also typical for CNG channels (Guo and Lu, 2000), but not for AMPARs (Bowie et al., 1998), which hints at a similar mechanism for TRPV and CNG channel block.

To explore a mechanism of spermine block of thermoTRPV channels, we therefore followed the modeling approach developed for PA inhibition and permeation of CNG channels (Guo and Lu, 2000). To account for the tri-phasic behavior of G_{rel}-V relationships, most obvious for TRPV1 and TRPV4 (Figs. 4 and 6), the model assumes two PA binding sites with different affinity, resulting in two blocked states without direct transitions between them (Fig. 5, B and C). PA can permeate when bound in conformation **a**, but not in conformation **b** (Fig. 5, B and C). We applied this model to the full concentration- and voltage-dependent spermine data on each of hTRPV1, 3, and 4, allowing the controlling rate constants and effective charges to vary between each channel, resulting in reasonably well predicted G_{rel}-V relationships for 10–1,000 µM spermine in each case (Fig. 6, solid lines, and Table 2). The equilibrium constants K_a and K_b, which reflect the steady state binding equilibria at the two sites, were quite similar for each channel. The constant K,
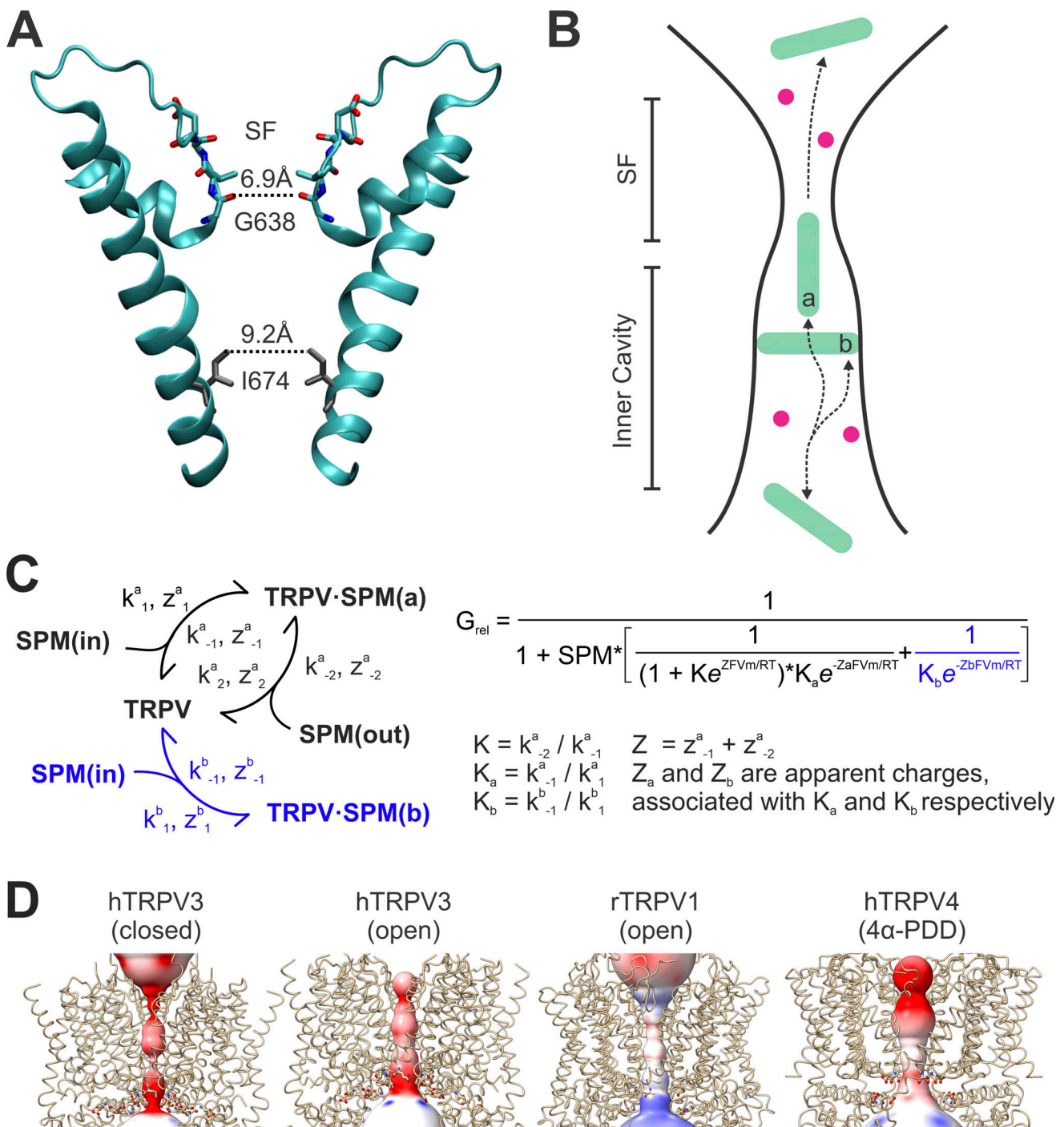
Figure 5. **Molecular model of TRPV inhibition by spermine. (A)** Human TRPV3 ion conduction pore (PDB accession no. 6UW6) with narrow regions: upper (6.9 Å) "gate" at the selectivity filter (SF) and lower (9.2 Å) gate in the cytoplasmic cavity. **(B)** Schematic of suggested model for spermine binding, blocking, and permeation. Green rods represent free spermine molecules and spermine bound in permeating (**a**) or non-permeating (**b**) conformations. Red circles represent metal cations (Na$^+$, K$^+$). **(C)** Kinetic model of TRPV inhibition by intracellular spermine. The model assumes either two (black and blue) or one (black only) spermine-bound states. Spermine can exit by permeation from only one state (TRPV · SP[a]). No direct transitions between the two bound states are allowed. Relative conductance (G$_{rel}$) is a function of cytoplasmic spermine concentration (SPM) and either six parameters (K, K$_a$, K$_b$, Z, Z$_a$, and Z$_b$) for the two-sites model or only four parameters (K, K$_a$, Z, and Z$_a$) for the one-site model. Parameter K represents the probability of spermine (bound in conformation **a**) permeating the channel versus going back to intracellular solution. Parameter K$_a$ represents the equilibrium dissociation constant of spermine bound in conformation **a**. **(D)** Pore electrostatic potentials of closed (PDB accession nos. 6UW4) and open (6UW6) hTRPV3, open rTRPV1 (5IRX), and hTRPV4 in presence of 4α-PDD (7AA5). Negatively charged (Glu) residues, localized to TM6–TRP helix linker are shown as sticks.
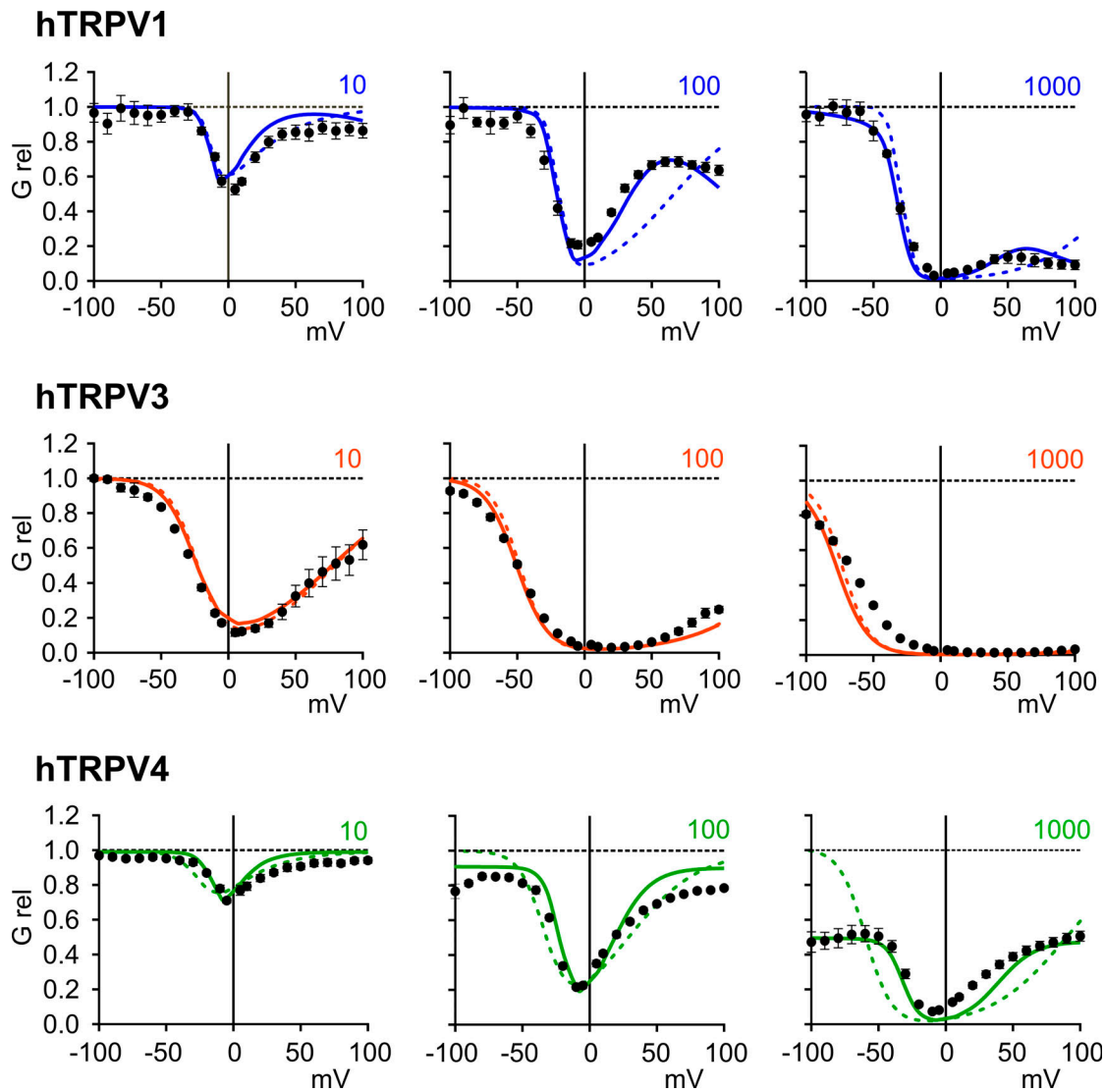
hTRPV1

hTRPV3

hTRPV4

Figure 6. **Kinetic model predictions of block and permeation.** G_{rel}-V in the presence of 10, 100, and 1,000 µM intracellular spermine was predicted by varying either six parameters (K, K_a, K_b, Z, Z_a, and Z_b, solid lines, two binding sites model) or four parameters (K, K_a, Z, and Z_a, dashed lines, one binding site model) for each of TRPV1, 3, and 4 channels are shown. Model curves are plotted superimposed on experimental data (same datasets as in Fig. 2 D and Fig. 4). The results of fitting with the two binding sites model are presented in Table 2.

which reflects the relative probability of spermine bound in conformation **a** permeating the channel versus going back to the intracellular solution, was approximately one order of magnitude lower for TRPV3 than TRPV1 or TRPV4, indicating higher permeability in the latter. Although the data sets were not sufficient to warrant formal modeling of the block by spermidine or putrescine, the same model is also likely to predict the results, with lower binding affinities, and potentially higher permeation rates for these smaller polyamines.

We also tested a one-site model, assuming only one PA binding site (conformation **a** in Fig. 5 C) described by the same equations as in Fig. 5 C without the term K_b (labeled in blue). Although this simplified model fit the data reasonably well in the case of TRPV3, it did not describe the inhibition of TRPV1 and TRPV4 (Fig. 6, dotted lines), and was therefore rejected as too simple.

Discussion

Expressed in both the central and peripheral nervous systems, TRPV1–4 are involved in the regulation of a multitude of physiological processes, including heat sensation, thermoregulation, itch, pain perception, and nociception, but also in immune response and (neuro)inflammation, osmoregulation, mechanotransduction, and bone formation. TRPV channel open probability, conductance, and ion selectivity, are extensively modulated by a number of parameters, including lipids (Lukacs et al., 2013; Cao et al., 2013), phosphorylation (Chung et al., 2008), and hydroxylation (Karttunen et al., 2014), as well as the extent of activation and even the type of agonist (Chung et al., 2008). We demonstrate here that each of TRPV1, 3, and 4 is effectively inhibited by physiological concentrations (Watanabe et al., 1991; Bowie and Mayer, 1995) of the endogenous intracellular PA spermine. We showed that this inhibition is concentration- and

Table 2. **The values of K, K$_a$, K$_b$, Z, Z$_a$, and Z$_b$ at various spermine concentrations obtained from fitting the data presented in Fig. 2 D and Fig. 4 using the kinetic model from Fig. 5 C**

	hTRPV1	hTRPV3	hTRPV4
K	7.9	1.1	10.5
K$_a$	$1.6 \cdot 10^{-6}$	$8.8 \cdot 10^{-7}$	$2.8 \cdot 10^{-6}$
K$_b$	$2.0 \cdot 10^{-3}$	$1.5 \cdot 10^{-3}$	$9.4 \cdot 10^{-4}$
Z	6.8	3.2	6.0
Z$_a$	5.1	2.5	4.2
Z$_b$	0.7	0.4	0.01

Two binding sites model was used, as shown in Fig. 6 (solid lines).

voltage-dependent, and is maximal around the reversal potential. Given extensive TRPV representation in excitable membranes, such non-linear voltage-dependent inhibition could be a powerful modulator, in particular during action potentials. Although a number of natural and synthetic agonists and inhibitors have been identified for TRPVs, so far, no voltage-dependent modulators are available. The steeply voltage-dependent PA block that we identify here thus introduces a potentially very dynamic and flexible regulatory mechanism.

Although total cellular PA content is estimated to be in the millimolar range, most intracellular PAs are bound to negatively charged macromolecules, including DNA, RNA, ATP, lipids, and proteins. Free spermine has been estimated to be in the 10–100 µM range, and other PAs at slightly higher concentrations, depending on the cell type (Watanabe et al., 1991; Bowie and Mayer, 1995). Although normally stable, intracellular PA content may be significantly altered in pathological conditions, including cancer (Li et al., 2020; Miska et al., 2021) and Alzheimer's disease (Morrison and Kish, 1995; Seidl et al., 1996; Inoue et al., 2013). As we show, at a likely physiological concentration of 10 µM, spermine provides significant inhibition of each of TRPV1, 3, and 4, with maximal block of 20–80% at membrane potentials around 0 mV. Additional, albeit weaker, contributions of other endogenous intracellular PAs, spermidine, and putrescine, typically present at concentrations similar to or higher than, spermine, will further add to the physiological action.

The behavior of each of TRPV1, 3, and 4 in the presence of spermine was similar to that previously reported for TRPC channels (Kim et al., 2016, 2020), which may imply a common (or a similar) mechanism throughout the TRP channel superfamily. CNG channels and ionotropic glutamate receptors are also inhibited by endogenous PAs with similar efficacy (Lu and Ding, 1999; Guo and Lu, 2000; Bowie and Mayer, 1995; Bähring et al., 1997; Bowie et al., 1998) and are also weakly permeable for PAs (Guo and Lu, 2000), as is TRPV1 (Ahern et al., 2006) and, probably, TRPV2 (Zubcevic et al., 2018b; Elbaz et al., 2016). Intracellular PA block of Kir channels (Lopatin et al., 1994; Lopatin et al., 1995) is typically much more potent, and there is much less evidence of permeation, potentially as a consequence of the much wider selectivity filter in TRPVs (Guo and Lu, 2003; Xu et al., 2009; Deng et al., 2018; Deng et al., 2020), although there

is evidence for some degree of block relief at positive voltages in both Kir2 and Kir4 channels (Guo and Lu, 2003; Kucheryavykh et al., 2007; Nichols and Lee, 2018).

There is no obvious relief from block by the bulky analog NASPM at 100 µM and much less complete relief at 10 or 1 µM than is seen for spermine. This is consistent with relief from spermine block being the result of spermine permeation, with NASPM being more restricted in traversing the narrowest regions of the pore, but some relief is consistent with previous data indicating that TRPV1 and TRPV2 are capable of conducting relatively large organic cations (Ahern et al., 2006; Chung et al., 2008; Li et al., 2011; Puopolo et al., 2013; Munns et al., 2015; Elbaz et al., 2016; Zubcevic et al., 2018b), including spermine in the case of TRPV1 (Ahern et al., 2006). The weaker block relief in TRPV3 at high depolarizing potentials implies a lower permeability of TRPV3 to spermine compared to the other TRPVs. Together with variable steepness of the G$_{rel}$-V relationships of TRPVs in the blocking phase, this feature suggests there will be different specific contributions of each TRPV sub-type to action potential properties.

The overall similarity of the G$_{rel}$-V relationships in TRPVs (Fig. 2 D and Fig. 4) and CNG channels, as well as their similar dependence on PA length and charge (Lu and Ding, 1999; Guo and Lu, 2000), suggests a common mechanism of PA block and relief. A similar mechanism of interaction is also consistent with the demonstration that both CNG channels and, at least, TRPV1 channels are capable of conducting polyamine molecules (Ahern et al., 2006). This prompted us to consider the same kinetic model suggested earlier for CNG channels (Lu and Ding, 1999; Guo and Lu, 2000). With two blocking sites, from only one of which the blocker may continue to permeate, the model provides a reasonably accurate description of spermine block, relief, and permeation for each of TRPV1, 3, 4 channels. The apparent binding affinities for spermine are similar in each channel, there is a much slower apparent exit rate of spermine to the outside in TRPV3. The model however does not imply any specific locations for spermine binding within the TRPV pore. As recent molecular dynamics analyses of strong inward rectifier Kir2 channels have suggested (Chen et al., 2020; Jogini et al., 2023; Lee and Nichols, 2023), polyamines may occupy a diffuse space within channel pores. Available structures of TRPV1, 3, and 4 (Fig. 5 D) indicates multiple regions of electronegativity along TRPV pores. The overall higher electronegativity of the entire length of TRPV3 conductive pore, particularly near the lower gate (Fig. 5 D), correlates with the higher polyamine sensitivity of this channel, and may contribute to its lower polyamine permeation rate.

Acknowledgments

References

Ahern, G.P., X. Wang, and R.L. Miyares. 2006. Polyamines are potent ligands for the capsaicin receptor TRPV1. *J. Biol. Chem.* 281:8991–8995. https://doi.org/10.1074/jbc.M513429200

Bähring, R., D. Bowie, M. Benveniste, and M.L. Mayer. 1997. Permeation and block of rat GluR6 glutamate receptor channels by internal and external polyamines. *J. Physiol.* 502:575–589. https://doi.org/10.1111/j.1469-7793.1997.575bj.x

Bowie, D., and M.L. Mayer. 1995. Inward rectification of both AMPA and kainate subtype glutamate receptors generated by polyamine-mediated ion channel block. *Neuron.* 15:453–462. https://doi.org/10.1016/0896-6273(95)90049-7

Bowie, D., G.D. Lange, and M.L. Mayer. 1998. Activity-dependent modulation of glutamate receptors by polyamines. *J. Neurosci.* 18:8175–8185. https://doi.org/10.1523/JNEUROSCI.18-20-08175.1998

Cao, E., J.F. Cordero-Morales, B. Liu, F. Qin, and D. Julius. 2013. TRPV1 channels are intrinsically heat sensitive and negatively regulated by phosphoinositide lipids. *Neuron.* 77:667–679. https://doi.org/10.1016/j.neuron.2012.12.016

Casero, R.A., Jr, T. Murray Stewart, and A.E. Pegg. 2018. Polyamine metabolism and cancer: Treatments, challenges and opportunities. *Nat. Rev. Cancer.* 18:681–695. https://doi.org/10.1038/s41568-018-0050-3

Caterina, M.J., M.A. Schumacher, M. Tominaga, T.A. Rosen, J.D. Levine, and D. Julius. 1997. The capsaicin receptor: A heat-activated ion channel in the pain pathway. *Nature.* 389:816–824. https://doi.org/10.1038/39807

Chen, X., M. Bründl, T. Friesacher, and A. Stary-Weinzinger. 2020. Computational insights into voltage dependence of polyamine block in a strong inwardly rectifying K⁺ channel. *Front. Pharmacol.* 11:721. https://doi.org/10.3389/fphar.2020.00721

Chung, M.-K., A.D. Güler, and M.J. Caterina. 2008. TRPV1 shows dynamic ionic selectivity during agonist stimulation. *Nat. Neurosci.* 11:555–564. https://doi.org/10.1038/nn.2102

Deng, Z., N. Paknejad, G. Maksaev, M. Sala-Rabanal, C.G. Nichols, R.K. Hite, and P. Yuan. 2018. Cryo-EM and x-ray structures of TRPV4 reveal insight into ion permeation and gating mechanisms. *Nat. Struct. Mol. Biol.* 25:252–260. https://doi.org/10.1038/s41594-018-0037-5

Deng, Z., G. Maksaev, M. Rau, Z. Xie, H. Hu, J.A.J. Fitzpatrick, and P. Yuan. 2020. Gating of human TRPV3 in a lipid bilayer. *Nat. Struct. Mol. Biol.* 27:635–644. https://doi.org/10.1038/s41594-020-0428-2

Dever, T.E., and I.P. Ivanov. 2018. Roles of polyamines in translation. *J. Biol. Chem.* 293:18719–18729. https://doi.org/10.1074/jbc.TM118.003338

Elbaz, M., D. Ahirwar, Z. Xiaoli, X. Zhou, M. Lustberg, M.W. Nasser, K. Shilo, and R.K. Ganju. 2016. TRPV2 is a novel biomarker and therapeutic target in triple negative breast cancer. *Oncotarget.* 9:33459–33470. https://doi.org/10.18632/oncotarget.9663

Ferreira, L.G.B., and R.X. Faria. 2016. TRPing on the pore phenomenon: What do we know about transient receptor potential ion channel-related pore dilation up to now? *J. Bioenerg. Biomembr.* 48:1–12. https://doi.org/10.1007/s10863-015-9634-8

Fleidervish, I.A., L. Libman, E. Katz, and M.J. Gutnick. 2008. Endogenous polyamines regulate cortical neuronal excitability by blocking voltage-gated Na⁺ channels. *Proc. Natl. Acad. Sci. USA.* 105:18994–18999. https://doi.org/10.1073/pnas.0803464105

Guo, D., and Z. Lu. 2000. Mechanism of cGMP-gated channel block by intracellular polyamines. *J. Gen. Physiol.* 115:783–798. https://doi.org/10.1085/jgp.115.6.783

Guo, D., and Z. Lu. 2003. Interaction mechanisms between polyamines and IRK1 inward rectifier K⁺ channels. *J. Gen. Physiol.* 122:485–500. https://doi.org/10.1085/jgp.200308890

Humphrey, W., A. Dalke, and K. Schulten. 1996. VMD: Visual molecular dynamics. *J. Mol. Graph.* 14:33–38. https://doi.org/10.1016/0263-7855(96)00018-5

Igarashi, K., and K. Kashiwagi. 2019. The functional role of polyamines in eukaryotic cells. *Int. J. Biochem. Cell Biol.* 107:104–115. https://doi.org/10.1016/j.biocel.2018.12.012

Inoue, K., H. Tsutsui, H. Akatsu, Y. Hashizume, N. Matsukawa, T. Yamamoto, and T. Toyo'oka. 2013. Metabolic profiling of Alzheimer's disease brains. *Sci. Rep.* 3:2364. https://doi.org/10.1038/srep02364

Jogini, V., M.Ø. Jensen, and D.E. Shaw. 2023. Gating and modulation of an inward-rectifier potassium channel. *J. Gen. Physiol.* 155:e202213085. https://doi.org/10.1085/jgp.202213085

Juvin, V., A. Penna, J. Chemin, Y.-L. Lin, and F.-A. Rassendren. 2007. Pharmacological characterization and molecular determinants of the activation of transient receptor potential V2 channel orthologs by 2-aminoethoxydiphenyl borate. *Mol. Pharmacol.* 72:1258–1268. https://doi.org/10.1124/mol.107.037044

Karttunen, S., M. Duffield, N.R. Scrimgeour, L. Squires, W.L. Lim, M.L. Dallas, J.L. Scragg, J. Chicher, K.A. Dave, M.L. Whitelaw, et al. 2014. Oxygen-dependent hydroxylation by factor inhibiting HIF (FIH) regulates the TRPV3 ion channel. *J. Cell Sci.* 128:225–231. https://doi.org/10.1242/jcs.158451

Kim, J., S.H. Moon, Y.-C. Shin, J.-H. Jeon, K.J. Park, K.P. Lee, and I. So. 2016. Intracellular spermine blocks TRPC4 channel via electrostatic interaction with C-terminal negative amino acids. *Pflugers Arch.* 468:551–561. https://doi.org/10.1007/s00424-015-1753-x

Kim, J., S.H. Moon, T. Kim, J. Ko, Y.K. Jeon, Y.-C. Shin, J.-H. Jeon, and I. So. 2020. Analysis of interaction between intracellular spermine and transient receptor potential canonical 4 channel: Multiple candidate sites of negatively charged amino acids for the inward rectification of transient receptor potential canonical 4. *Korean J. Physiol. Pharmacol.* 24: 101–110. https://doi.org/10.4196/kjpp.2020.24.1.101

Koike, M., M. Iino, and S. Ozawa. 1997. Blocking effect of 1-naphthyl acetyl spermine on Ca²⁺-permeable AMPA receptors in cultured rat hippocampal neurons. *Neurosci. Res.* 29:27–36. https://doi.org/10.1016/S0168-0102(97)00067-9

Kucheryavykh, Y.V., W.L. Pearson, H.T. Kurata, M.J. Eaton, S.N. Skatchkov, and C.G. Nichols. 2007. Polyamine permeation and rectification of Kir4.1 channels. *Channels.* 1:172–178. https://doi.org/10.4161/chan.4389

Lee, S.-J., and C.G. Nichols. 2023. Seeing spermine blocking of K⁺ ion movement through inward rectifier Kir2.2 channels. *J. Gen. Physiol.* 155: e202213144. https://doi.org/10.1085/jgp.202213144

Li, H., S. Wang, A.Y. Chuang, B.E. Cohen, and H.H. Chuang. 2011. Activity-dependent targeting of TRPV1 with a pore-permeating capsaicin analog. *Proc. Natl. Acad. Sci. USA.* 108:8497–8502. https://doi.org/10.1073/pnas.1018550108

Li, J., Y. Meng, X. Wu, and Y. Sun. 2020. Polyamines and related signaling pathways in cancer. *Cancer Cell Int.* 20:539. https://doi.org/10.1186/s12935-020-01545-9

Liedtke, W., Y. Choe, M.A. Martí-Renom, A.M. Bell, C.S. Denis, A. Sali, A.J. Hudspeth, J.M. Friedman, and S. Heller. 2000. Vanilloid receptor-related osmotically activated channel (VR-OAC), a candidate vertebrate osmoreceptor. *Cell.* 103:525–535. https://doi.org/10.1016/S0092-8674(00)00143-4

Lopatin, A.N., E.N. Makhina, and C.G. Nichols. 1994. Potassium channel block by cytoplasmic polyamines as the mechanism of intrinsic rectification. *Nature.* 372:366–369. https://doi.org/10.1038/372366a0

Lopatin, A.N., E.N. Makhina, and C.G. Nichols. 1995. The mechanism of inward rectification of potassium channels: "long-pore plugging" by cytoplasmic polyamines. *J. Gen. Physiol.* 106:923–955. https://doi.org/10.1085/jgp.106.5.923

Lu, Z., and L. Ding. 1999. Blockade of a retinal cGMP-gated channel by polyamines. *J. Gen. Physiol.* 113:35–43. https://doi.org/10.1085/jgp.113.1.35

Lukacs, V., J.-M. Rives, X. Sun, E. Zakharian, and T. Rohacs. 2013. Promiscuous activation of transient receptor potential vanilloid 1 (TRPV1) channels by negatively charged intracellular lipids: The key role of endogenous phosphoinositides in maintaining channel activity. *J. Biol. Chem.* 288:35003–35013. https://doi.org/10.1074/jbc.M113.520288

Marrone, M.C., A. Morabito, M. Giustizieri, V. Chiurchiù, A. Leuti, M. Mattioli, S. Marinelli, L. Riganti, M. Lombardi, E. Murana, et al. 2017. TRPV1 channels are critical brain inflammation detectors and neuropathic pain biomarkers in mice. *Nat. Commun.* 8:15292. https://doi.org/10.1038/ncomms15292

Méndez-González, M.P., Y.V. Kucheryavykh, A. Zayas-Santiago, W. Vélez-Carrasco, G. Maldonado-Martínez, L.A. Cubano, C.G. Nichols, S.N. Skatchkov, and M.J. Eaton. 2016. Novel KCNJ10 gene variations compromise function of inwardly rectifying potassium channel 4.1. *J. Biol. Chem.* 291:7716–7726. https://doi.org/10.1074/jbc.M115.679910

Minois, N., D. Carmona-Gutierrez, and F. Madeo. 2011. Polyamines in aging and disease. *Aging.* 3:716–732. https://doi.org/10.18632/aging.100361

Miska, J., A. Rashidi, C. Lee-Chang, P. Gao, A. Lopez-Rosas, P. Zhang, R. Burga, B. Castro, T. Xiao, Y. Han, et al. 2021. Polyamines drive myeloid cell survival by buffering intracellular pH to promote immunosuppression in glioblastoma. *Sci. Adv.* 7:eabc8929. https://doi.org/10.1126/sciadv.abc8929

Morrison, L.D., and S.J. Kish. 1995. Brain polyamine levels are altered in Alzheimer's disease. *Neurosci. Lett.* 197:5–8. https://doi.org/10.1016/0304-3940(95)11881-V

Munns, C.H., M.-K. Chung, Y.E. Sanchez, L.M. Amzel, and M.J. Caterina. 2015. Role of the outer pore domain in transient receptor potential vanilloid 1 dynamic permeability to large cations. *J. Biol. Chem.* 290: 5707–5724. https://doi.org/10.1074/jbc.M114.597435

Neeper, M.P., Y. Liu, T.L. Hutchinson, Y. Wang, C.M. Flores, and N. Qin. 2007. Activation properties of heterologously expressed mammalian TRPV2: Evidence for species dependence. *J. Biol. Chem.* 282: 15894–15902. https://doi.org/10.1074/jbc.M608287200

Nichols, C.G., and S.J. Lee. 2018. Polyamines and potassium channels: A 25-year romance. *J. Biol. Chem.* 293:18779–18788. https://doi.org/10.1074/jbc.TM118.003344

Nilius, B., J. Prenen, T. Voets, and G. Droogmans. 2004. Intracellular nucleotides and polyamines inhibit the Ca^{2+}-activated cation channel TRPM4b. *Pflugers Arch.* 448:70–75. https://doi.org/10.1007/s00424-003-1221-x

Nilius, B., T. Bíró, and G. Owsianik. 2014. TRPV3: Time to decipher a poorly understood family member!. *J. Physiol.* 592:295–304. https://doi.org/10.1113/jphysiol.2013.255968

Patapoutian, A., S. Tate, and C.J. Woolf. 2009. Transient receptor potential channels: Targeting pain at the source. *Nat. Rev. Drug Discov.* 8:55–68. https://doi.org/10.1038/nrd2757

Pegg, A.E. 2016. Functions of polyamines in mammals. *J. Biol. Chem.* 291: 14904–14912. https://doi.org/10.1074/jbc.R116.731661

Peier, A.M., A.J. Reeve, D.A. Andersson, A. Moqrich, T.J. Earley, A.C. Hergarden, G.M. Story, S. Colley, J.B. Hogenesch, P. McIntyre, et al. 2002. A heat-sensitive TRP channel expressed in keratinocytes. *Science.* 296: 2046–2049. https://doi.org/10.1126/science.1073140

Perálvarez-Marín, A., P. Doñate-Macian, and R. Gaudet. 2013. What do we know about the transient receptor potential vanilloid 2 (TRPV2) ion channel?. *FEBS J.* 280:5471–5487. https://doi.org/10.1111/febs.12302

Pettersen, E.F., T.D. Goddard, C.C. Huang, E.C. Meng, G.S. Couch, T.I. Croll, J.H. Morris, and T.E. Ferrin. 2021. UCSF ChimeraX: Structure visualization for researchers, educators, and developers. *Protein Sci.* 30:70–82. https://doi.org/10.1002/pro.3943

Puopolo, M., A.M. Binshtok, G.-L. Yao, S.B. Oh, C.J. Woolf, and B.P. Bean. 2013. Permeation and block of TRPV1 channels by the cationic lidocaine derivative QX-314. *J. Neurophysiol.* 109:1704–1712. https://doi.org/10.1152/jn.00012.2013

Sánchez-Jiménez, F., M.Á. Medina, L. Villalobos-Rueda, and J.L. Urdiales. 2019. Polyamines in mammalian pathophysiology. *Cell. Mol. Life Sci.* 76: 3987–4008. https://doi.org/10.1007/s00018-019-03196-0

Saiki, S., Y. Sasazawa, M. Fujimaki, K. Kamagata, N. Kaga, H. Taka, Y. Li, S. Souma, T. Hatano, Y. Imamichi, et al. 2019. A metabolic profile of polyamines in Parkinson disease: A promising biomarker. *Ann. Neurol.* 86:251–263. https://doi.org/10.1002/ana.25516

Seidl, R., S. Beninati, N. Cairns, N. Singewald, D. Risser, H. Bavan, M. Nemethova, and G. Lubec. 1996. Polyamines in frontal cortex of patients with Down syndrome and Alzheimer disease. *Neurosci. Lett.* 206: 193–195. https://doi.org/10.1016/S0304-3940(96)12451-4

Singh, A.K., L.L. McGoldrick, and A.I. Sobolevsky. 2018. Structure and gating mechanism of the transient receptor potential channel TRPV3. *Nat. Struct. Mol. Biol.* 25:805–813. https://doi.org/10.1038/s41594-018-0108-7

Skatchkov, S.N., M.A. Woodbury-Fariña, and M. Eaton. 2014. The role of glia in stress: Polyamines and brain disorders. *Psychiatr. Clin. North Am.* 37: 653–678. https://doi.org/10.1016/j.psc.2014.08.008

Skatchkov, S.N., S.M. Antonov, and M.J. Eaton. 2016. Glia and glial polyamines. Role in brain function in health and disease. *Biochem. (Mosc.) Suppl. Ser. A. Membr. Cell Biol.* 10:73–98. https://doi.org/10.1134/S1990747816010116

Smith, G.D., M.J. Gunthorpe, R.E. Kelsell, P.D. Hayes, P. Reilly, P. Facer, J.E. Wright, J.C. Jerman, J.-P. Walhin, L. Ooi, et al. 2002. TRPV3 is a temperature-sensitive vanilloid receptor-like protein. *Nature.* 418: 186–190. https://doi.org/10.1038/nature00894

Strotmann, R., C. Harteneck, K. Nunnenmacher, G. Schultz, and T.D. Plant. 2000. OTRPC4, a nonselective cation channel that confers sensitivity to extracellular osmolarity. *Nat. Cell Biol.* 2:695–702. https://doi.org/10.1038/35036318

Tominaga, M., M.J. Caterina, A.B. Malmberg, T.A. Rosen, H. Gilbert, K. Skinner, B.E. Raumann, A.I. Basbaum, and D. Julius. 1998. The cloned capsaicin receptor integrates multiple pain-producing stimuli. *Neuron.* 21:531–543. https://doi.org/10.1016/S0896-6273(00)80564-4

Twomey, E.C., M.V. Yelshanskaya, A.A. Vassilevski, and A.I. Sobolevsky. 2018. Mechanisms of channel block in calcium-permeable AMPA receptors. *Neuron.* 99:956–968.e4. https://doi.org/10.1016/j.neuron.2018.07.027

Watanabe, S., K. Kusama-Eguchi, H. Kobayashi, and K. Igarashi. 1991. Estimation of polyamine binding to macromolecules and ATP in bovine lymphocytes and rat liver. *J. Biol. Chem.* 266:20803–20809. https://doi.org/10.1016/S0021-9258(18)54780-3

White, J.P.M., M. Cibelli, L. Urban, B. Nilius, J.G. McGeown, and I. Nagy. 2016. TRPV4: Molecular conductor of a diverse orchestra. *Physiol. Rev.* 96: 911–973. https://doi.org/10.1152/physrev.00016.2015

Xu, Y., H.-G. Shin, S. Szép, and Z. Lu. 2009. Physical determinants of strong voltage sensitivity of K^+ channel block. *Nat. Struct. Mol. Biol.* 16: 1252–1258. https://doi.org/10.1038/nsmb.1717

Yang, F., L. Xu, B.H. Lee, X. Xiao, V. Yarov-Yarovoy, and J. Zheng. 2020. An unorthodox mechanism underlying voltage sensitivity of TRPV1 ion channel. *Adv. Sci.* 7:2000575. https://doi.org/10.1002/advs.202000575

Yuan, P. 2019. Structural biology of thermoTRPV channels. *Cell Calcium.* 84: 102106. https://doi.org/10.1016/j.ceca.2019.102106

Zhelay, T., K.B. Wieczerzak, P. Beesetty, G.M. Alter, M. Matsushita, and J.A. Kozak. 2018. Depletion of plasma membrane-associated phosphoinositides mimics inhibition of TRPM7 channels by cytosolic Mg^{2+}, spermine, and pH. *J. Biol. Chem.* 293:18151–18167. https://doi.org/10.1074/jbc.RA118.004066

Zubcevic, L., M.A. Herzik Jr., M. Wu, W.F. Borschel, M. Hirschi, A.S. Song, G.C. Lander, and S.-Y. Lee. 2018a. Conformational ensemble of the human TRPV3 ion channel. *Nat. Commun.* 9:4773. https://doi.org/10.1038/s41467-018-07117-w

Zubcevic, L., S. Le, H. Yang, and S.-Y. Lee. 2018b. Conformational plasticity in the selectivity filter of the TRPV2 ion channel. *Nat. Struct. Mol. Biol.* 25: 405–415. https://doi.org/10.1038/s41594-018-0059-z